

## Conference Paper

# Manufacturing and characterization of epoxy resin with Fe<sub>3</sub>O<sub>4</sub> and SiO<sub>2</sub> particles

José Molina<sup>1</sup>, Bożena Szczucka-Lasota<sup>2</sup>, Tomasz Węgrzyn<sup>2</sup>, Abílio P. Silva<sup>1</sup>, and Alberto Maceiras<sup>1</sup>

<sup>1</sup>Centre For Mechanical and Aerospace Science and Technologies (C-MAST), Universidade da Beira Interior

<sup>2</sup>Silesian University of Technology, Transport Department

## Abstract

Thermosetting polymers are very popular in the automotive and aeronautic industry, in particular epoxy resin is widely used as matrix thermoset in carbon and glass fibre reinforced composites. The properties of these epoxy-based polymers can be improved with the addition of particulate or small fibre materials in order to construct a lightweight material with enhanced mechanical and structural response. This work aimed to manufacture and characterize epoxy resin reinforced composites with iron (II, III) oxide (magnetite, Fe<sub>3</sub>O<sub>4</sub>) in amounts of 0.25, 0.5 and 1 wt%, and 2 and 4 wt% of fumed silicon dioxide (silica, SiO<sub>2</sub>). Mechanical properties were investigated by three-point bending flexural test, fracture toughness, flexural stress relaxation. In addition, apparent porosity, apparent density and Differential Scanning Calorimetry tests were performed. The results showed that the addition of Fe<sub>3</sub>O<sub>4</sub> does not contribute significantly to the improvement of mechanical properties. However, fumed SiO<sub>2</sub> promotes a considerable improvement in the mechanical properties.

Corresponding Author:

José Molina

jose.francisco.garcia@ubi.pt

Received: 26 November 2019

Accepted: 13 May 2020

Published: 2 June 2020

Publishing services provided by  
Knowledge E

© José Molina et al. This article is distributed under the terms of the [Creative Commons Attribution License](#), which permits unrestricted use and redistribution provided that the original author and source are credited.

Selection and Peer-review under the responsibility of the ICEUBI2019 Conference Committee.

**Keywords:** Composite, epoxy resin, Fe<sub>3</sub>O<sub>4</sub>, SiO<sub>2</sub>, mechanical properties

## 1. Introduction

Thermosetting polymers are very popular in the automotive and aeronautic industry. In this group, the epoxy resin family can be highlighted. Based on their low shrinkage, high strength and good durability in warm and moist environments they are the most used in aircraft structures. Despite that, epoxies cannot be safely used inside cabins due to poor fire performance, because they ignite in an easy way and release a large amount of heat and smoke [1]. Other thermosets are also used, such as bismaleimides (BMIs), phenolic-triazine resins or polybenzoxazine [2]. Some properties of these thermosetting polymers are summarized in Table 1. It is observed that epoxy resins do not outstand for any of their properties, but it is the combination of all of them that makes them an “all-rounder” [2].

### OPEN ACCESS

TABLE 1: Properties of several thermosets (adapted from [2])

	Epoxy	Phenolic	Toughened BMI	Phenolic-triazine	Poly-benzoxazine
Tensile strength (MPa)	90-120	24-25	50-90	4.2	100-125
Tensile modulus (GPa)	3.1-3.8	3-5	3.5-4.5	4.1	3.8-4.5
Glass transition temperature ( $T_g$ )(°C)	150-220	170	230-280	300-400	170-340
Max. temperature of service (°C)	180	200	200	300	130-280
Density (g/cm <sup>3</sup> )	1.2-1.25	1.24-1.32	1.2-1.3	1.25	1.197
KIC (MPa·m <sup>1/2</sup> )	0.6	1.01	0.85	0.2-0.3	0.6-1.1

Since the 1990s, the use of composites, especially fiber-reinforced composites, has increased in the aeronautical industry, competing nowadays with aluminium alloys in order to be the dominant material. The main reasons for that are the reduction of weight, the increase of strength and stiffness, the reduction of corrosion issues, and the diminution in the number of components (specially the number of joints).

Epoxy resins are widely used in aeronautics as adhesives or as the matrix of a composite material. However, in order to improve their properties and enlarge the scope of applications, these resins are usually reinforced. Usually, the addition of fillers, in particular ceramic particles, aims to upgrade mechanical and thermal properties, and if possible, others such as electrical or magnetic properties, looking for an additional characteristic as functional or multifunctional materials.

Bazrgari *et al.* [3] studied the addition of 1 vol.% of Al<sub>2</sub>O<sub>3</sub> nanoparticles into epoxy resin improves the flexural strength (>15%), stiffness and impact strength, whereas the wear rate and friction coefficient decreased. Furthermore, Y. Chen *et al.* [4] analysed the influence of the addition of  $\alpha$ -Al<sub>2</sub>O<sub>3</sub> nanoparticles in the electrical insulation of an epoxy composite. The results showed an improvement of the DC volume resistivity from  $9.4 \times 10^{17}$  to  $2.2 \times 10^{18}$   $\Omega \cdot \text{cm}$  at 30°C.

Eskizeybek *et al.* [5] observed the influence of CaCO<sub>3</sub> nanofillers in epoxy and carbon fiberreinforced carbon (CFRC) matrices. For a 2 wt% of CaCO<sub>3</sub> increments in tensile strength (22.2% and 48.4% for the epoxy and CFRC, respectively), toughness (37% and 78.6% for the epoxy and CFRC, respectively), flexural load (53.4% and 46.8% for the epoxy and CFRC, respectively) were detected. Furthermore, there was an improvement of the critical threshold forces of the CFRC of 16.8%, 13.4% and 11.3% for 2m/s, 2.5m/s and 3m/s respectively.

S.K. Singh *et al.* [6] added TiO<sub>2</sub> micro and nanoparticles observing an improvement in the tensile strength and ductility, being this improvement higher for a 4 wt% of NPs

(43.7% in tensile strength). It also showed an improvement of the fracture energy (GIC) and an increase of 142% in the fracture toughness ( $K_{IC}$ ).

The addition of iron (III) oxide ( $Fe_2O_3$ ) carried out by T. Sun et al. [7] showed that for an epoxy resin filled with a 4 wt% of  $Fe_2O_3$  the tensile strength improved in a 50% while fracture toughness ( $K_{IC}$ ) improved in a 106%.

Rajadurai A. et al. [8] reported that the addition of  $Fe_2O_3$  particles improves the tensile, flexural and impact strength and the thermal stability by 55.4%, 9.7%, 23.9% and 36%, respectively.

A. Radón et al. [9] studied the electrical properties of an epoxy composite containing  $Fe_3O_4$  nanoparticles reporting an improvement in the electromagnetic interference shielding and the microwave absorption properties, and high activation and hopping energy.

Moreover, N. Saleh et al. [10] observed the behaviour of an epoxy resin with the addition of fly ash and fumed silica. The results showed that the presence of both fillers improved compression and tensile strength, whereas the addition of fumed silica alone improved impact strength but suffering a loss in bending and hardness strength. Furthermore, by adding solely fly ash improved hardness strength but the impact strength decreased.

A. H. Majeed [11] added fumed silica experimenting an improvement in hardness, compression strength and wave transmission velocity of a 2 wt%. Furthermore, A. Christy et al. [12] added silicon dioxide ( $SiO_2$ ) up to 3 wt% and reported an improvement in tensile and impact properties. S. K. Singh et al. [13] carried out a similar study, but with higher percentages (up to 8 wt%). Their results showed that, for 4 wt% of  $SiO_2$  an improvement of 31%, 17% and 76% in its tensile strength, flexural strength and flexural modulus, respectively. For higher weight percentages of  $SiO_2$  the values started to decrease.

This work aims to contribute to the improvement of the manufacturing procedure of epoxy matrices with particulate additive in order to obtain superior properties. It is also intended to characterize the properties of composites and compare them with the literature in order to discuss improvements in the methodology. In this context is described the manufacturing, mixing and curing processes of a common epoxy resin (Epoxy resin SR 8100) with the addition of two fillers: fumed  $SiO_2$  and  $Fe_3O_4$  nanoparticles. The effect in several properties, such as flexural properties, stress relaxation, toughness, apparent density and porosity, and glass transition temperature ( $T_g$ ) was examined.

## 2. Experimental Procedure

Epoxy resin SR 8100 combined with the hardener SD 8824 both provided by Sicomin were used. As fillers, iron oxide ( $\text{Fe}_3\text{O}_4$ ) provided by Fisher Scientific and fumed  $\text{SiO}_2$  provided by Aldrich Chemistry were employed.

Table 2 summarizes the experimental apparent density ( $\rho$ ) and the average value of the particle size distribution ( $D_{50}$ ) of the materials.

TABLE 2: Properties of the resin and filler materials

Material	$\rho(\text{g/cm}^3)$	$D_{50}(\mu\text{m})$
Epoxy resin SR 8100	1.158	-
Hardener SD 8824	0.944	-
$\text{Fe}_3\text{O}_4$	5.180	1.055
Fumed $\text{SiO}_2$	0.368	0.007

Table 3 summarizes the main mechanical and the glass transition temperature of the cured epoxy resin with the hardener, after a curing cycle of 24 hours at room temperature and a post curing treatment of 24 hours at  $40^\circ\text{C}$ , provided by the supplier [14].

TABLE 3: Properties of the epoxy resin cured (SR 8100/SD 8824) [14].

Tensile strength (MPa)	60
Tensile modulus (MPa)	2900
Flexural strength (MPa)	108
Flexural modulus (MPa)	3000
$T_g$ ( $^\circ\text{C}$ )	63

The obtained initial samples had square shape obtained from a square plate mould of 140mm x 140mm.  $\text{Fe}_3\text{O}_4$  particles were mixed with epoxy resin in the weight percentages of 0.25, 0.5 and 1 wt.%, and fumed  $\text{SiO}_2$  particles also in the weight percentages of 2 and 4 wt.%. The fillers were added into the resin, mixed with a mechanical mixer from Lbx instruments at 1000 rpm for 3 hours, and dispersed at the same time with an ultrasonic bath, GT Sonic. The temperature of the bath was controlled with ice to prevent overheating. Following, in order to minimize the air bubbles produced during the mixing, each epoxy-filler mixture was introduced in a vacuum chamber, Baco Eng, for three periods of 30 minutes. After that, the hardener was added in a 100/22 weight ratio and hand-mixed for 10 minutes using a glass rod. Then, the mixture was poured into the mould, and left first 24 hours at room temperature and later 24 hours more at  $40^\circ\text{C}$  in order to complete the curing process.

To determine the density (specific mass) and the apparent porosity, the Archimedes' principle was used (ASTM C20, adapted). The density ( $\rho$ ), in  $[\text{g}/\text{cm}^3]$  was obtained following Eq.(1).

$$\rho = \frac{D_w}{V_e} \quad (1)$$

where " $D_w$ " is the dry weight,  $V_e$  is the exterior volume calculated by Eq.(2).

$$V_e = W - S \quad (2)$$

where " $W$ " is the saturated weight and " $S$ " is the suspended weight. Furthermore, the apparent porosity ( $P_A$ ) is calculated by Eq.(4).

$$P_A = \frac{W - D_w}{V_e} \cdot 100 \quad (3)$$

In order to analyze the glass transition temperature ( $T_g$ ) samples of cylindrical shape with 6 mm of diameter and 1 mm of thickness were analyzed employing differential scanning calorimetry (DSC) (Netzsch DSC 204) with a constant heating rate of  $10^\circ\text{C}/\text{min}$  up to  $150^\circ\text{C}$  under nitrogen atmosphere. Three tests were performed for each composite.

To perform the mechanical tests, the plates were cut using a Struers Accutom-2, in order to obtain parallelepipedic samples with dimensions of  $10\text{mm} \times 75\text{mm} \times 2.2\text{mm}$ . For the flexural stress and strain three-point bending tests were conducted in the universal testing machine Shimadzu AGS-X following the ASTM D790 method. At least 5 different specimens of each type of sample were tested with a span ( $L$ ) of  $40\text{mm}$  and a crosshead motion rate of  $1.1\text{ mm}/\text{min}$ . Flexural tests ( $\sigma$ ), calculated by the Eq.(4), were determined from the load of the applied force ( $P$ ) a function of geometric factors (width,  $b$ , and thickness  $d$ ).

$$\sigma = \frac{3PL}{2bd^2} \quad (4)$$

The strain ( $\epsilon$ ) was calculated by the Eq.(5) using the deflection at the center of the beam ( $D$ ) along the elapsed time.

$$\epsilon = \frac{6Dd}{L^2} \quad (5)$$

Stress relaxation tests were performed in order to analyse the viscoelastic behaviour of the specimens with  $0.25\text{ wt.}\% \text{ Fe}_3\text{O}_4$  and  $4\text{ wt.}\% \text{ SiO}_2$ , and the unreinforced epoxy resin as control material, during periods of applied stress of 3 hours, employing 80% of the maximum stress determined previously in the flexural tests.

Additionally, with the objective of analysing the fracture toughness ( $K_{IC}$ ), some single edge notch bend (SENB) tests were performed, following the ASTM D5045 standard

test. Beams with a pre-crack were made by lightly tapping a fresh razor blade between adjoining plates, yielding a very sharp natural crack. To carry out the tests, six different specimens of each were tested in the testing machine Shimadzu AGS-X, with 3-point bending configuration, span 4 times the value of  $W$  (20 mm) and rate of 10 mm/min. The output of these tests was the fracture toughness ( $K_{IC}$ ) calculated by the Eq.(6).

$$K_{IC} = \frac{P_b}{BW^{1/2}} f(x) \tag{6}$$

where " $P_b$ " is the load at the breaking point, " $B$ " is the thickness " $W$ " is the width and the " $f(x)$ " is determined by the Eq.(7).

$$f(x) = 6(x)^{1/2} \frac{[1.9 - x(1 - x)(2.15 - 3.93x) + 2.72x^2]}{(1 + 2x)(1 - x)^{3/2}} \tag{7}$$

where " $x$ " is the crack length divided by the width, i.e. ( $a/W$ ). In view of the very low conductivity of the samples, their morphology characterization by scanning electron microscopy (SEM) was difficult to perform and the quality of the results deficient. SEM gave an acceptable local view on samples and an overall view of the sample. The accumulation of electric charge on the surface prevented the use of EDX to characterise the distribution of the fillers and the composition measurement of the particles. However, it is not possible to study, in detail, the interface quality among the particles and the resin matrix.

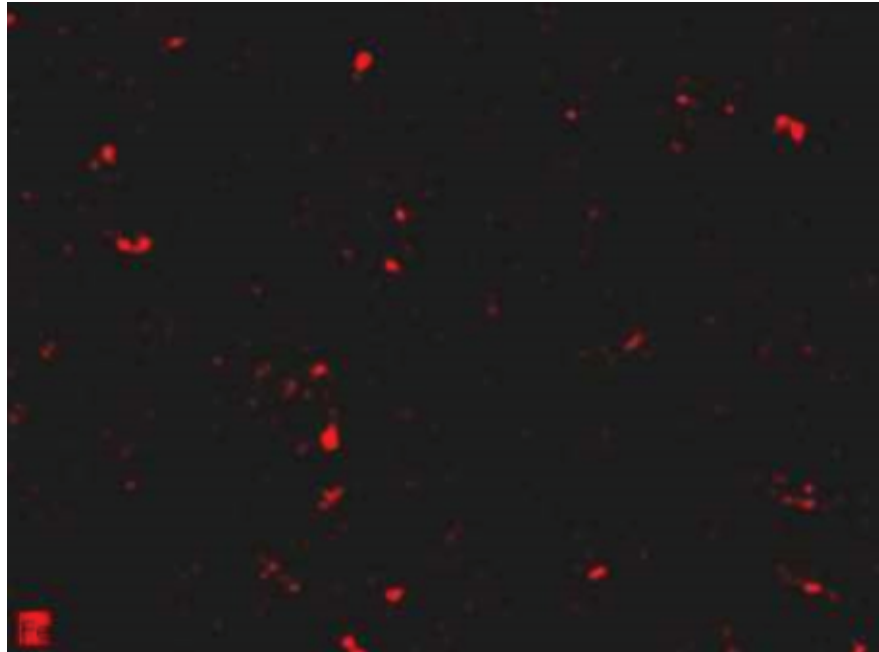
### 3. Results and Discussion

Figure 1 and Figure 2 show the SEM-EDX mapping of the  $Fe_3O_4$  and  $SiO_2$  composites, respectively.

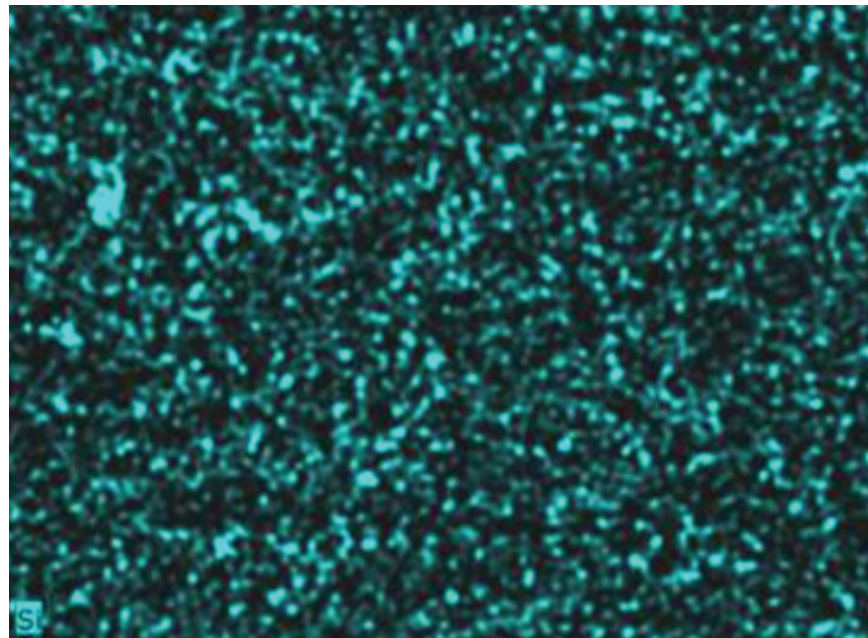
From the observation of both images, a homogeneous particle distribution with the presence of a few clusters can be perceived. The final manufactured product quality of the different  $Fe_3O_4$  composites was good, but for the  $SiO_2$  composites some air bubbles are observed. In Table 4, the apparent density ( $\rho$ ), the apparent porosity ( $P_A$ ) and the relative density ( $\rho_r$ ) results are shown.

TABLE 4: Density and apparent porosity of the  $Fe_3O_4$  and  $SiO_2$  doped epoxy composites.

	Fe <sub>3</sub> O <sub>4</sub> (wt.%)			Fumed SiO <sub>2</sub> (wt.%)	
	0.25	0.50	1.00	2.00	4.00
$\rho$ (g/cm <sup>3</sup> )	1.17	1.19	1.18	1.19	1.19
$P_A$ (%)	0.51	0.29	0.49	0.35	0.28
$\rho_r$	0.99	1.00	1.00	0.95	0.91



**Figure 1:** SEM-EDX mapping of epoxy doped with 1 wt.% of  $\text{Fe}_3\text{O}_4$  composites



**Figure 2:** SEM-EDX mapping of the epoxy-based composites doped with 2 wt.% of fumed  $\text{SiO}_2$ .

The specimens obtained from the epoxy resin filled with  $\text{Fe}_3\text{O}_4$  and  $\text{SiO}_2$  had a density very similar with the unfilled resin ( $1.158 \text{ g/cm}^3$ ) due to a relatively low porosity (lower than 1%). In order to evaluate the influence of manufacturing defects, the relative density ( $\rho_r$ ) i.e. the ratio between the experimental density ( $\rho$ ,  $\text{g/cm}^3$ ) and the theoretical density ( $\rho_{th}$ ,  $\text{g/cm}^3$ , obtained by the phase mixture rule), was determined. The relative density observed was very high (true porosity less than 1%) for  $\text{Fe}_3\text{O}_4$  composites. However, the

true porosity is 5% and 9% for composites reinforced by 2 and 4% of SiO<sub>2</sub>, respectively. This closed porosity may influence the characterization of these composites. Thus, a correction model of Rice, Eq.(8) [15] is used to minimize the porosity effect in the mechanical properties.

$$X = X_0 \cdot e^{-3P} \quad (8)$$

where “X” is the real property, “X<sub>0</sub>” is the property for zero porosity and “P” is the true porosity.

In Table 5 the glass transition temperatures for all composites are summarized. The Standard ASTM E1356 test method for determining the glass transition temperatures by differential scanning calorimetry distinguishes three different “temperatures” or transition points associated with the glass transition region. The first one is the onset temperature, which is the point of intersection of the tangent drawn at the point of greatest slope on the transition curve with the extrapolated baseline prior to the transition. The second one is the inflection temperature that is the point on the thermal curve corresponding to the peak of the first derivative of the parent thermal curve. And finally, the end temperature, which is the point of intersection of the tangent drawn at the point of greatest slope on the transition curve with the extrapolated baseline following the transition.

TABLE 5: Glass transition temperature for the composites.

	Epoxy	Fe <sub>3</sub> O <sub>4</sub> (wt%)			SiO <sub>2</sub> (wt%)	
	0	0.3	0.5	1.0	2.0	4.0
Onset T <sub>g</sub> (°C)	63.2	58.4	58.5	53.3	61.6	59.1
Inflection T <sub>g</sub> (°C)	64.2	59.4	60.4	55.2	62.0	60.4
End T <sub>g</sub> (°C)	66.0	59.7	67.1	55.7	63.1	61.9

The results for the control samples (epoxy resin) were validated with the information provided by the supplier ( $T_g = 63^\circ\text{C}$ ). Moreover, the experimental results for the nanocomposites showed a tendency to decrease. The explanation can be related to a poor interfacial interaction among the particles and the matrix, as stated by Jordan et al. [16]. The maximum stress ( $\sigma_{max}$ ), the strain at this point ( $\epsilon_{max}$ ) and the Young's modulus value of each specimen are summarized in Table 6. In order to evaluate the porosity effect in SiO<sub>2</sub> reinforced composites the Eq.(8) was applied and the estimated values presented into parentheses.

It can be observed that, for the low Fe<sub>3</sub>O<sub>4</sub> percentage composites the value of  $\sigma_{max}$  decreases slightly (107 to 106 MPa) and more largely for higher filler percentages. On the other hand, for the SiO<sub>2</sub> composites,  $\sigma_{max}$  increases significantly (from 107 to 131

TABLE 6: Flexural properties of the composites.

	Epoxy	Fe <sub>3</sub> O <sub>4</sub> (wt%)			SiO <sub>2</sub> (wt%)	
	0.0	0.3	0.5	1.0	2.0	4.0
$\sigma_{max}$ (MPa)	107 ± 3	106 ± 0.3	106 ± 2	98 ± 5	131 ± 3 (152)	124 ± 3 (162)
$\epsilon_{max}$ (%)	5.0 ± 0.04	4.7 ± 0.19	5.2 ± 0.12	4.9 ± 0.26	4.7 ± 0.26	4.8 ± 0.07
Young's modulus (GPa)	2.81 ± 0.1	2.95 ± 0.2	2.62 ± 0.2	2.50 ± 0.1	3.48 ± 0.5 (4.04)	3.41 ± 0.1 (4.47)
$K_{IC}$ (MPa.m <sup>1/2</sup> )	2.1 ± 0.1	2.2 ± 0.1	2.1 ± 0.1	2.0 ± 0.1	2.3 ± 0.2 (2.7)	2.2 ± 0.2 (2.9)

MPa). In the case of the Young's modulus, the value increases when either of the two fillers is added, being the maximum value at 0.25% for the Fe<sub>3</sub>O<sub>4</sub> and 2% for the SiO<sub>2</sub> composition. If the zero porosity is estimated applying the Eq.(8), the addition of 4 wt.% of SiO<sub>2</sub> considerably increases the value of the maximum stress (51%) and Young's modulus (59%).

For SiO<sub>2</sub> the strain at  $\sigma_{max}$  decreases smoothly, but for the Fe<sub>3</sub>O<sub>4</sub> has a minimum at 0.25%, corresponding to the maximum modulus, and then oscillates around 5%.

The fracture toughness ( $K_{IC}$ ) characterizes the resistance of a material to fracture in the presence of a sharp crack under a severe tensile constraint. The values obtained are also summarized in Table 6. The  $K_{IC}$  value is not influenced by the Fe<sub>3</sub>O<sub>4</sub> particles, but the addition of SiO<sub>2</sub> increases the fracture toughness, i.e. the relation between failure stress and defect size is higher, especially if zero porosity is estimated.

After normalizing the data obtained for  $\sigma_{max}$  to compare the influence of both fillers in stress relaxation terms, the stress values are converted to non-dimensional values by dividing them by the 80% of the maximum value of stress. The evolution of stress plotted in a graph representing the evolution of the stress along the time. This evolution is shown in Figure 3. The control of epoxy resin specimens showed a relaxation of 25%, while the samples of 0.25 wt.% Fe<sub>3</sub>O<sub>4</sub> and 4 wt.% SiO<sub>2</sub> showed a decrease of 25% and 23%, respectively. These values show an improvement in stress relaxation, but in a very slightly way.

## 4. Conclusion

The manufacturing process quality of the composites reinforced by Fe<sub>3</sub>O<sub>4</sub> is very good, with true porosity less than 1%, which indicates good homogeneity (Figure 1), few clusters and good interface quality. The addition of SiO<sub>2</sub> fumed particles presented

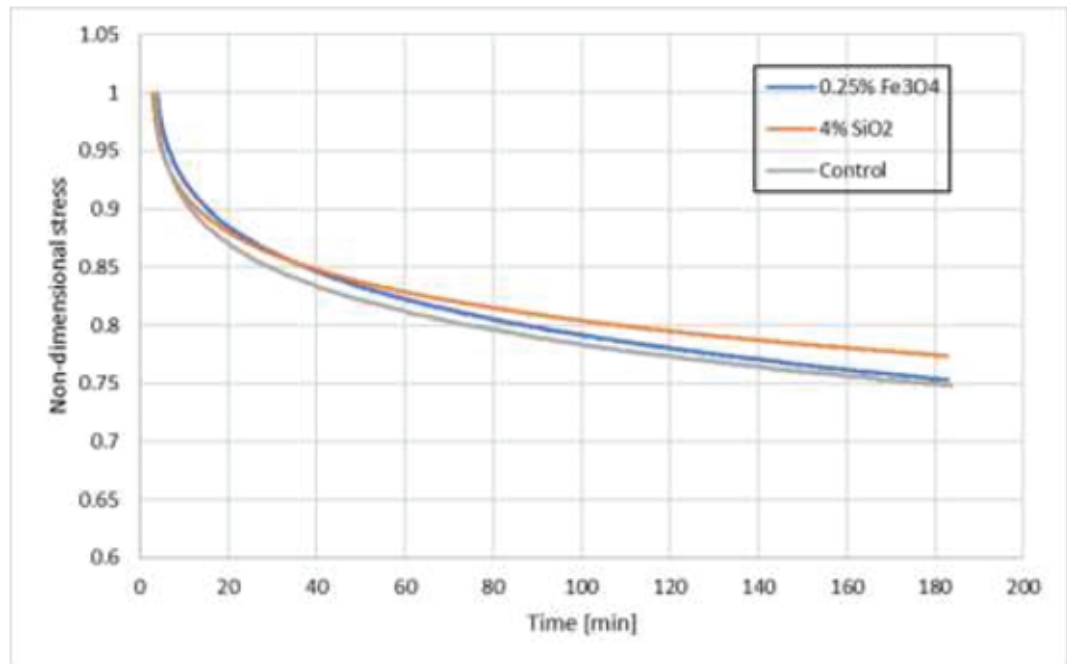


**Figure 3:** Stress relaxation of the 0.25wt% Fe<sub>3</sub>O<sub>4</sub> and 4wt% SiO<sub>2</sub> composites in comparison with epoxy resin (control)

an obstacle due to its low density, high viscosity during the mixing process, which leads to a higher porosity (5% and 9%). Nevertheless, some conclusions are quite evident from the characterization, namely:

- Glass transition temperature ( $T_g$ ) decrease with the addition of either fillers.
- With the addition of Fe<sub>3</sub>O<sub>4</sub> particles the maximum stress remains constant. However, for a 0.25 wt.% there is a slight improvement in the Young's modulus (5%),  $K_{IC}$  presents a small increase (1%), and a reduction in the strain (6%).
- With the addition of fumed SiO<sub>2</sub> particles, there is an improvement in the experimental values of  $t\sigma_{max}$  and Young's modulus for 2 wt.% (22% and 24%, respectively), a reduction in the strain of a 6%, and the  $K_{IC}$  value increases a 9%. This improvement is verified even with a true porosity of 5%. Thus, using the correction model Eq. (8) to estimate the values for zero porosity, the addition of 4% of SiO<sub>2</sub> increases considerably the value of the maximum stress (51% higher) and Young's modulus (59% higher).
- The experimental stress relaxation of the resin suffers a mild improvement when adding Fe<sub>3</sub>O<sub>4</sub> and SiO<sub>2</sub> particles, but this improvement is no significant.

In conclusion, the addition of fumed SiO<sub>2</sub>, especially as manufacturing conditions are improved with resulting to obtain true zero porosity, promotes a considerable

improvement in mechanical properties. Nonetheless, the addition of  $\text{Fe}_3\text{O}_4$  does not significantly contribute to the mechanical properties' improvement.

## Acknowledgements

This work was supported by the project Centro-01-0145-FEDER-000017 - EMaDeS - Energy, Materials and Sustainable Development, co-financed by the Portugal 2020 Program (PT 2020), within the Regional Operational Program of the Center (CENTRO 2020) and the European Union through the European Regional Development Fund (ERDF).

## References

- [1] Mouritz A. P. (2012). *Polymers for aerospace structures. Introduction to Aerospace Materials*. Cambridge: Woodhead Publishing.
- [2] Hamerton I. and Kratz J. (2018). The use of thermosets in modern aerospace applications. *Thermosets*. Bristol: Elsevier.
- [3] Bazgari, D., Moztarzadeh, F., Sabbagh-Alvani, A., et al (2018). Mechanical properties and tribological performance of epoxy/ $\text{Al}_2\text{O}_3$  nanocomposite. *Ceramics International*, vol. 44, issue 1, pp. 1220-1224.
- [4] Chen, Y., Zhang, D., Wu, X, et al (2017). Epoxy/ $\alpha$ -alumina nanocomposite with high electrical insulation performance. *Progress in Natural Science: Materials International*, vol. 27 issue 5, pp 574-581.
- [5] Eskizeybek, V., Ulus, H., Kaybal, H.B., et al (2018). Static and dynamic mechanical responses of  $\text{CaCO}_3$  nanoparticle modified epoxy/carbon fiber composite. *Composites Part B: Engineering*, vol. 140 issue 1, pp. 223-231.
- [6] Singh, S. K., Singh, S., Kumar, A., and Jain, A. (2017). Thermo-mechanical behaviour of  $\text{TiO}_2$  dispersed epoxy composites. *Engineering Fracture Mechanics*, vol. 184, issue 15, pp. 241-248.
- [7] Sun, T., Fan, H., Wang, Z., et al (2015). Modified nano  $\text{Fe}_2\text{O}_3$ -epoxy composite with enhanced mechanical properties. *Materials and Design*, vol. 87, issue 15, pp. 10-16.
- [8] Arun Prakash, V. R. and Rajadurai, A. (2016). Thermo-mechanical characterization of siliconized Eglass fiber/hematite particles reinforced epoxy resin hybrid composite. *Applied Surface Science*, vol. 384, issue 30, pp. 99-106.
- [9] Radoń, A., Włodarczyk, P., Drygała, A., and Łukowiec, D. (2019). Electrical properties of epoxy nanocomposites containing  $\text{Fe}_3\text{O}_4$  nanoparticles and  $\text{Fe}_3\text{O}_4$  nanoparticles

deposited on the surface of electrochemically exfoliated and oxidized graphite. *Applied Surface Science*, vol. 474, issue 30, pp. 66-77.

- [10] Saleh N. and Al-Maamori, M. H. (2014). Evaluating the mechanical properties of Epoxy resin with Fly ash and Silica fume as fillers. *Advances in Physics Theories and Applications*, vol. 30.
- [11] Majeed A. H. (2018). Enforcement of epoxy with silica fume and carbon fiber. *Tikrit Journal of Engineering Sciences*, vol. 25, issue 1, pp. 74-77.
- [12] Christy, A., Purohit, R., Rana, R. S. *et al* (2017). Development and Analysis of Epoxy/nano SiO<sub>2</sub> Polymer Matrix Composite fabricated by Ultrasonic Vibration assisted Processing. *Materials Today: Proceedings*, vol. 4, issue 2, pp. 2748-2754.
- [13] Singh, S. K.; Kumar, A., and Jain, A. (2018). Improving tensile and flexural properties of SiO<sub>2</sub>-epoxy polymer nanocomposite. *Materials Today: Proceedings*, vol 5, issue 2, pp. 6339-6344.
- [14] Sicomin Epoxy Systems (2019). SR 8100/SD 882X Infusion System. *E1436 Data Sheet*.
- [15] Rice, R.W (1998). *Porosity of Ceramics*. New York: Marcel Dekker. P. 102.
- [16] Jordan, J., Jacob, K. I., Tannenbaum, R., *et al*. (2005). Experimental trends in polymer nanocomposites - a review. *Materials Science and Engineering: A*, vol. 393, issue 1-2, pp. 1-11.